ACS Medicinal Chemistry Letters

Letter

pubs.acs.org/acsmedchemlett

Discovery of a Potent Analgesic NOP and Opioid Receptor Agonist: Cebranopadol

Stefan Schunk,*[,†] Klaus Linz,[‡] Claudia Hinze,[†] Sven Frormann,[†] Stefan Oberbörsch,[†] Bernd Sundermann,[†] Saskia Zemolka,[†] Werner Englberger,[§] Tieno Germann,[§] Thomas Christoph,[∥] Babette-Y. Kögel,[∥] Wolfgang Schröder,[∥] Stephanie Harlfinger,[⊥] Derek Saunders,[⊥] Achim Kless,[#] Hans Schick,[○] and Helmut Sonnenschein[○]

[†]Departments of Medicinal Chemistry, [‡]Preclinical Drug Safety, [§]Molecular Pharmacology, [∥]Pain Pharmacology, [⊥]Pharmacokinetics, and [#]Discovery Informatics, Global Drug Discovery, Grünenthal Innovation, Grünenthal GmbH, D-52099 Aachen, Germany

[○]ASCA GmbH Angewandte Synthesechemie Adlershof, Magnusstr. 11, 12489 Berlin, Germany

Supporting Information

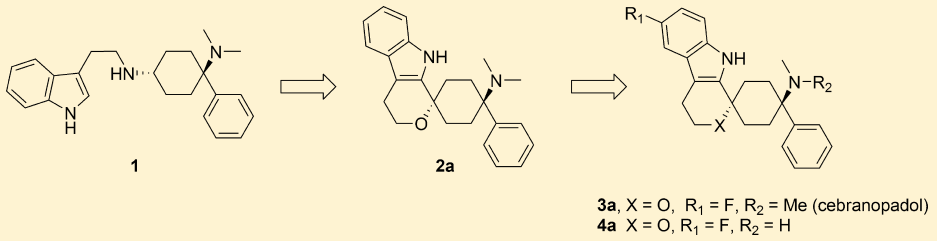

ABSTRACT: In a previous communication, our efforts leading from **1** to the identification of spiro[cyclohexane-dihydropyrano[3,4-*b*]indole]-amine **2a** as analgesic NOP and opioid receptor agonist were disclosed and their favorable in vitro and in vivo pharmacological properties revealed. We herein report our efforts to further optimize lead **2a**, toward *trans*-6′-fluoro-4′,9′-dihydro-*N*,*N*-dimethyl-4-phenyl-spiro[cyclohexane-1,1′(3′*H*)-pyrano[3,4-*b*]indol]-4-amine (cebranopadol, **3a**), which is currently in clinical development for the treatment of severe chronic nociceptive and neuropathic pain.

KEYWORDS: *NOP receptor agonists, MOP receptor agonists, cebranopadol, analgesics*

Recent publications indicate that small molecules activating both nociceptin/orphanin FQ peptide (NOP) and mu opioid peptide (MOP) receptors may potentiate opiate analgesia and at the same time display an improved side effects profile.[1,2] We have recently reported the discovery of a series of small molecules, characterized by their high NOP and opioid receptor agonistic activity.[3] This series included uncyclized (e.g., **1**) as well as spirocyclic examples (e.g., **2a**). The discovery of spirocyclic **2a** originated from the respective uncyclized analogues, which were potent NOP and MOP receptor binders but sometimes hampered by only partial agonistic NOP and MOP receptor activity. In particular, the spiroindole derivates sparked our interest due to their structural novelty and favorable in vitro and in vivo properties. The leading spiroether **2a** exhibited strong efficacy in preclinical models of acute (ED_{50} rat tail-flick: 3.63 nmol/kg i.v.) and neuropathic pain (ED_{50} rat spinal nerve ligation: 1.05 nmol/kg i.v.) but was hampered by poor pharmacokinetic (PK) properties in rats with high clearance, large volume of distribution, moderate half-life (Cl = 4.0 L/h·kg; V_{ss} = 7.52 L/kg; $t_{1/2}$ = 1.6 h), and a critically very low oral bioavailability (F = 4%).

We herein report our efforts to further optimize the spiroindole lead **2a**, which eventually led to the discovery of *trans*-6′-fluoro-4′,9′-dihydro-*N*,*N*-dimethyl-4-phenyl-spiro-[cyclohexane-1,1′(3′*H*)-pyrano[3,4-*b*]indol]-4-amine (**3a**, cebranopadol), a novel potent analgesic NOP and opioid receptor agonist, currently in clinical development for the treatment of severe chronic nociceptive and neuropathic pain.

The structure−activity relationship (SAR) established around the uncyclized scaffolds (e.g., **1**) suggested that a broad variety of linkers such as alcohols, ethers, and amines are tolerated, showing high NOP and MOP receptor binding affinities.[3] As a result, we applied this knowledge through analogous structural variations to lead structure **2a** (region A, Figure 1). These changes were also combined with a targeted approach to improve the poor PK profile, in particular by addressing metabolically liable regions B and C.

With this in mind, the transformation of the oxacyclic spiro moiety into a carba-, aza-, or thio-cyclic moiety was investigated. Advancing from the oxacyclic spiro **2a** to the azacyclic moiety **5a** led to equally potent NOP and MOP receptor binders, as well as the introduction of the *N*-methyl subunit **6a**. Similarly, potency was retained when moving from the oxa-cycle **2a** to the thio-cycle **7a** and carbacycle **8a** (Table 1).

Received: March 19, 2014
Accepted: June 12, 2014
Published: June 24, 2014

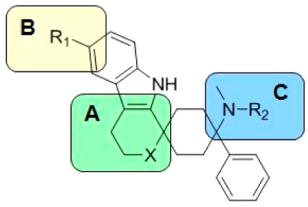

Figure 1. Sites of modification.

Table 1. Modification of Spirocyclic Oxygen, Region A

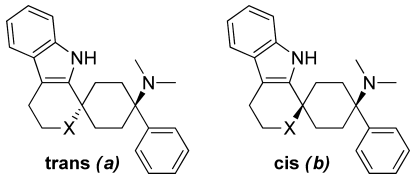

			% inhibition @ 1 μM or K_i (nM)	
compd	X	config	*h*NOPr	*h*MOPr
2a[b]	O	trans	0.1	0.26
2b[b]	O	cis	30%	310
5a[c]	NH	trans	0.19	0.39
6a[c]	NMe	trans	0.55	0.24
7a[a]	S	trans	3.7	3.1
8a	CH_2	trans	1.26	1.95

[a]Hemicitrate. [b]Hydrochloride. [c]Dihydrochloride.

The wide range of tolerated moieties suggests that, upon cyclization, the molecule has been brought into a preferred conformation at both receptors (Figure 2). As a consequence of these results and employing the most favored core from a lipophilicity point of view, we focused our efforts for further optimization on the oxacyclic moiety.

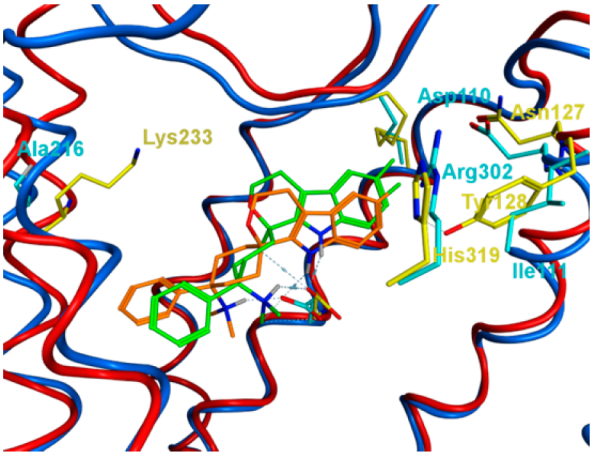

Figure 2. Three-dimensional structural overlay of the binding modes of **3a** in the NOP and MOP receptors. NOP: Binding modes of **3a** (orange) in the NOP receptor: NOP ribbons, blue; residues, cyan. MOP: Binding modes of **3a** (green) in the MOP receptor: MOP ribbons, red; residues, yellow. MOP ribbons of helix 7, His319/Arg302, removed for clarity.

The synthesis of chemotypes described in this letter is shown in Scheme 1. Tryptophol **9** or its TMS ether **10**, thiotryptophol **13**, and commercially available tryptamines **14** and **15** were cyclized with 4-dimethylamino-4-phenyl-cyclohexanone **19** to give the corresponding spirocycles **2**–**7** under similar conditions to the ones reported previously.[3]

To achieve carbacycle **8**, another route was necessary: 5-triethylsilyl-4-pentyn-1-ol **20** was converted into the corresponding iodide **21**, which after metal–halogen exchange with *t*BuLi was added to previously described[3] **19** to give **22**. Larock cyclization[4] of the triethylsilyl alkyne moiety with *ortho*-iodoaniline gave the indole-3-yl-propyl moiety in **23**.

After silyl deprotection with TBAF, spirocyclization of **24** was achieved with TMSOTf as promoter to give **8a** after separation from the accompanying cis diastereomer by HPLC.[5]

The spirocyclization of 4-methylamino-cyclohexanone **27** gave the corresponding *N*-monomethyl analogue **28a**.

Also cyclic amino heads, such as 4-phenyl-4-pyrrolidin-1-yl-cyclohexanone, were successfully synthesized and spirocyclized in analogous manner to give **38b**–**40b**.

As illustrated in our previous publication, compound **2a**, following intravenous administration, showed excellent efficacy in the rat tail-flick and spinal nerve ligation model while having a promising side effects profile. Nevertheless, it suffered from poor oral bioavailability and high clearance. To understand this further we subjected **2a** to metabolite ID. These investigations identified *N*-demethyl compound **28a** (Table 2) and 6′-hydroxy compound **48a** (Table 3) as metabolites in humans and rodents. Our optimization efforts therefore aimed at targeting both sites of metabolism to improve the PK profile.

The dimethyl amine head was tackled first. Synthesis of the *N*-demethyl metabolite, analogue **28a**, resulted in a compound with potent NOP and MOP receptor binding activity. For the cyclic amine heads piperidine **38b**, *N*-methyl piperazine **39b**, and morpholine **40b**, we only obtained the generally less active cis stereoisomer. However, because the introduction of cyclic amine heads resulted in complete loss of binding affinities, we concluded that there is little room for optimization here and retained the dimethylamino moiety for further optimization. We therefore turned our interest to the 6′-position of the indole spiro scaffold with the aim to block this point of metabolic instability.

As previously reported, the relative stereochemistry remained crucial for high NOP and MOP receptor binding affinities[3] with the trans stereoisomer being the favored stereoisomer with respect to binding affinity (**2a** vs **2b**; **3a** vs **3b**). This has been rationalized, through a bidentate, chelating binding mode to Asp130, which is only feasible from the trans configuration.[3]

Pleasingly, a variety of small substituents such as Me (**47a**), F (**3a**, **3b**, and **4a**), OH (**48a**), and OMe (**49a**) could be obtained by use of trytophols **41**–**43** and TMS ether **45** and were well tolerated by both receptors. Indeed, as described in Table 3, all trans stereoisomers demonstrated binding affinities below 20 nM at both the NOP and MOP receptor.

Despite the good receptor binding properties, we decided only to progress compounds with a NOP/MOP selectivity factor of <5, as our focus was for equipotent NOP and MOP receptor binders. On this basis, compounds **3a**, **4a**, **5a**, and **48a** were advanced into in vitro functional testing.

Equipotent binding at the MOP and NOP receptor was rationalized by overlaying the recently published crystal structures of the MOP and NOP receptors.[6,7] Major differences of the MOP and NOP receptor binding sites are Lys233 (MOP)/Ala216 (NOP), Asn127 (MOP)/Asp110 (NOP), His319 (MOP)/Arg302 (NOP), and Tyr128 (MOP)/Ile111 (NOP) switches (Figure 2).

dx.doi.org/10.1021/ml500117c | ACS Med. Chem. Lett. 2014, 5, 857–862

Scheme 1. Synthesis of Investigated Spirocycles[a]

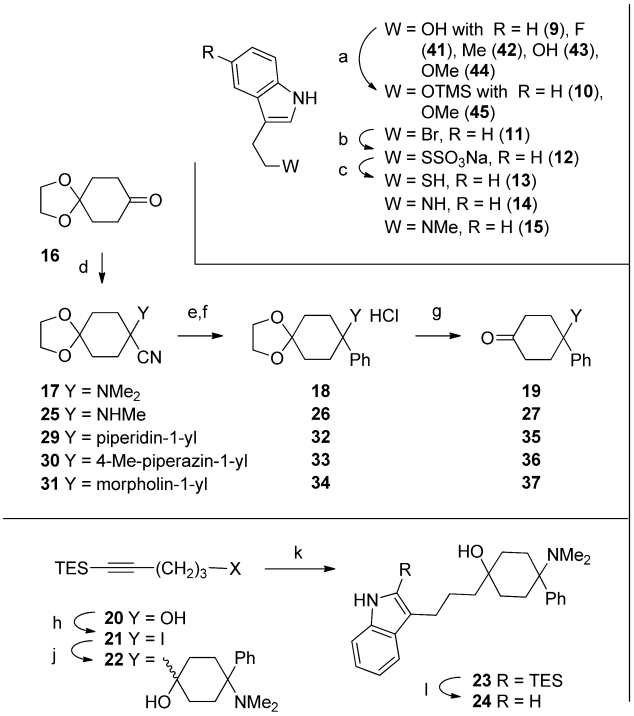

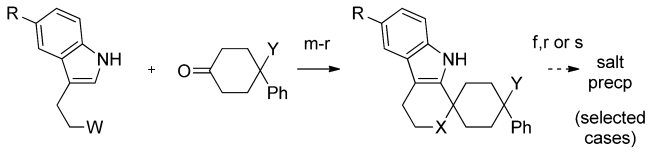

9-10, 13-15, 24, 41-43, 46 = Nu | **19, 27, 35-37** | **2-8, 28, 38-40, 47-49**

product	Nu	W	R	ketone	X	Y	cond[a]
2	**10**	OTMS	H	**19**	O	NMe_2	m,f
3a	**41**	OH	F	**19**	O	NMe_2	m,f
3b	**41**	OH	F	**19**	O	NMe_2	n,s
4	**41**	OTMS	F	**27**	O	NHMe	o,s
5	**14**	NH_2	H	**19**	NH	NMe_2	p,s
6	**15**	NHMe	H	**19**	NMe	NMe_2	p
7	**13**	SH	H	**19**	S	NMe_2	q,s
8	**24**	CH_2OH	H	**19**	CH_2	NMe_2	m
28	**9**	OTMS	H	**27**	O	NHMe	o,s
38	**9**	OH	H	**35**	O	piperidin-1-yl	r
39	**9**	OH	H	**36**	O	4-Me-piperazin-1-yl	r
40	**9**	OH	H	**37**	O	morpholin-1-yl	r
47	**43**	OH	Me	**19**	O	NMe_2	m,s
48	**44**	OH	OH	**19**	O	NMe_2	m,s
49	**46**	OTMS	OMe	**19**	O	NMe_2	o,s

[a]Reagents and conditions: (a) (i) $HN(TMS)_2$, TMSCl, THF; (ii) $NaHCO_3$, Et_2O, 88−100%; (b) (i) $Na_2S_2O_3$, H_2O, EtOH reflux; (ii) *i*-PrOH reflux, 75%; (c) 50 v/v H_3PO_4/H_2O, Et_2O, reflux, 96%; (d) (i) HY or 40 w/w $HNMe_2/H_2O$, MeOH, 4 N HCl, KCN, 0 °C to rt; (ii) H_2O, Et_2O, DCM, 84−97%; (e) (i) PhMgCl, THF, 0 °C to rt; (ii) NH_4Cl, H_2O, 0 °C to rt, Et_2O; (f) 2-butanone, TMSCl, 0 °C to rt, 35−58% over steps (e) and (f); (g) (i) 7.5 N HCl, Et_2O; (ii) NaOH, 78−97%; (h) 5-(TES)-4-pentin-1-ol, MeCN, Ph_3PI_2, imidazole, 70%; (j) (i) *t*-BuLi/pentane, Et_2O, −75 to −70 °C; (ii) **13**, Et_2O, 28%; (k) (i) iodoaniline, [1,3-bis(2,6-*i*-Pr_2Ph)-imidazol-2-ylidene]-(3-Cl-Py)Pd(II)-chloride, Na_2CO_3, DMF, 100 °C; (ii) $Na_2S_2O_3$, 66%; (l) TBAF, THF, reflux, 50 °C, 36%; (m) TMSOTf, DCM, rt, 33−99%; (n) (i) H_3PO_4, conc. AcOH; (ii) NaOH, 96%; (o) TfOH, DCM, rt; (ii) NaOH; (iii) MeOH, 65−67%; (p) TFA, DCE, 3−31%; (q) (i) TMSOMs, DCM, rt; (ii) filtration; (iii) evaporation filtrate, recryst EtOH; (iii) citric acid, EtOH, 65 °C to rt, 11% **7a**; (r) (i) MsOH, DCM; (ii) filtration, 63−99%; (s) citric acid, hot ethanol, 5 °C 12 h, 53−99%.

Table 2. Variation of the Amine Head, Region C

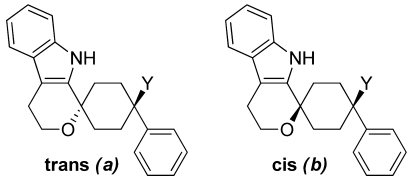

			% inhibition @ 1 μM or K_i (nM)	
compd	Y	config	*h*NOPr	*h*MOPr
2a[a]	NMe_2	trans	0.1	0.26
28a[b]	NHMe	trans	1.1	0.36
38b[c]	piperidin-1-yl	cis	<10%	43%
39b[d]	4-Me-piperazin-1-yl	cis	<10%	<10%
40b[c]	morpholin-2-yl	cis	<10%	<10%

[a]Hydrochloride. [b]Hemicitrate. [c]Methanesulfonate. [d]Dimethanesulfonate.

Table 3. Variation of Substituents at Major Metabolic Positions, Region B

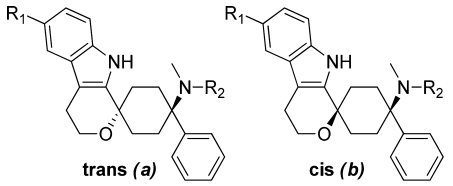

				% inhibition @ 1 μM or K_i (nM)	
compd	R^1	R^2	config	*h*NOPr	*h*MOPr
3a[a]	F	Me	trans	0.9	0.7
3b[a]	F	Me	cis	97.4	46
4a[a]	F	H	trans	11	2
47a[a]	Me	Me	trans	4.5	2.7
48a[a]	OH	Me	trans	1	0.4
49a[b]	OMe	Me	trans	9.4	1.1

[a]Hemicitrate. [b]Hydrochloride.

This should allow for similar pi−pi stacking interactions of aromatic moieties at the NOP and MOP receptors. Hydrophobic cavities are conserved in both receptors. We have subsequently docked compound **3a** in both receptors and observed only slightly different binding modes;[8] therefore, similar binding affinities at the NOP and MOP receptors are to be expected.

More detailed characterization of **3a** hemicitrate revealed binding affinities of 2.6 nM (N = 7, ± SD = 1.4) and 18.0 nM (N = 11, ± SD = 20.0 nM) at the *h*KOP and *h*DOP receptors.[9]

Functional investigations on **3a**, **4a**, **5a**, and **48a** revealed that all compounds acted as full agonists at both the MOP and NOP receptor and could therefore be progressed (Table 4). We

dx.doi.org/10.1021/ml500117c | ACS Med. Chem. Lett. 2014, 5, 857−862

nevertheless decided to drop **5a** because of concerns with regards to *h*ERG (data not shown).

Table 4. Functional Assay Results for Selected Compounds

	EC_{50} GTPγS (nM)		rel. eff.[a] GTPγS	
compd	*h*NOPr	*h*MOPr	*h*NOPr	*h*MOPr
3a[b]	13	1.2	89%	104%
4a[b]	60	2.6	101%	110%
5a[c]	1.3	0.2	108%	101%
48a[b]	120	1.2	75%	96%

[a]Efficacy of 100% is defined as maximum [^{35}S]GTPγS binding induced by stimulation with nociceptin (NOP receptor) and DAMGO (MOP receptor). [b]Hemicitrate. [c]Dihydrochloride.

After these promising in vitro results we progressed **3a**, **4a**, and **48a** into in vivo PK profiling. Compound **3a** showed good mouse PK properties with low clearance (Cl = 0.96 L/h·kg), moderate half-life ($t_{1/2}$ = 2.57 h), medium volume of distribution (V_c = 2.96 L/kg), and good oral bioavailability (F = 44%). In rats, **3a** achieved a significant improvement in oral bioavailability (F = 23%) as compared to **2a** (F = 4%).[3] The mouse PK of **4a** is characterized by a very high clearance (Cl = 15.3 L/h·kg), very high volume of distribution (V_z = 72.5 L/kg), longer half-life ($t_{1/2}$ = 3.50 h), and good oral bioavailability (F = 44%).

Compounds **3a**, **4a**, and **48a** were initially compared with regards to their activity in a mouse tail-flick model of acute nociceptive pain using a method modified from D'Amour and Smith.[10] Antinociceptive activity of the compounds was quantified after i.v. and p.o. dosing by measuring the increase in the latency for tail withdrawal from a radiant heat source in male NMRI mice[11] (Table 5). Compound **3a** induced dose-dependent inhibition of heat nociception with ED_{50} values of 40.1 nmol/kg i.v. and 77.0 nmol/kg p.o. (Figure 3 and Table 5). With both routes of administration, the maximum attainable antinociceptive response was obtained, indicating full antinociceptive efficacy.

In order to characterize the duration of analgesic action, equieffective dosages of the high dose range (>90% of the maximum possible effect (MPE)) were chosen. After oral administration, significant antinociceptive activity was observed for more than 8 h (last test point measured), where 85% MPE was still reached. The duration of action after intravenous administration lasted up to 3 h, where 38% MPE was measured.

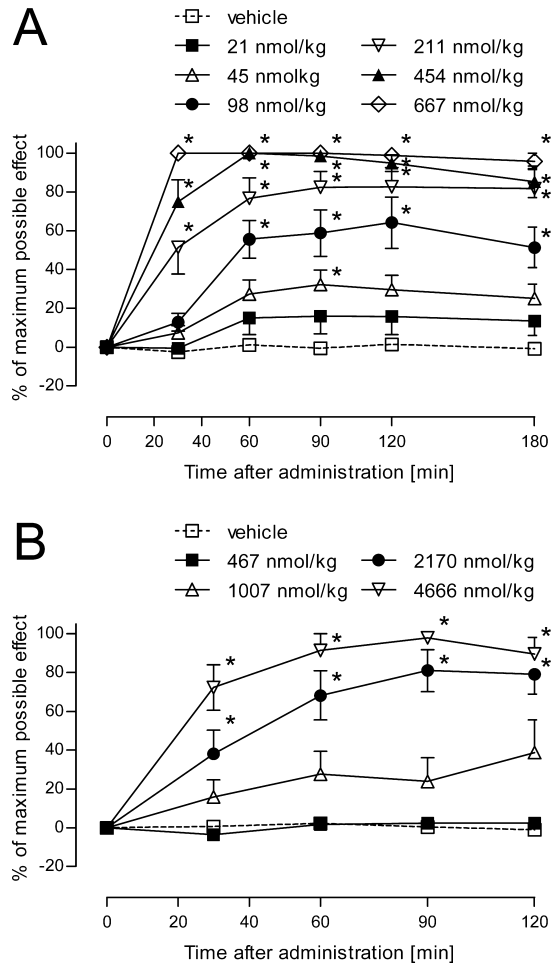

Figure 3. Mouse tail-flick test: Dose–response curves of cebranopadol (**3a**) hemicitrate (A) and **4a** hemicitrate (B) obtained after oral administration. Each point of the graph represents the mean ± SEM of the maximum possible effect (MPE); n = 10 animals per group. *p < 0.05 versus vehicle.

These investigations demonstrate that **3a** is highly effective in an animal model of acute nociceptive pain. It is about as equipotent to the strong opioid fentanyl citrate but shows a significantly longer duration of action and, in contrast to fentanyl, displays high potency and long lasting efficacy as well after oral administration (see Table 5).

Table 5. In Vivo Results for Selected Compounds in a Mouse Tail-Flick Model of Acute Nociceptive Pain

	tail-flick mouse		
compd	ED_{50} (95% CI) [nmol/kg]	E_{max} (%MPE)	duration of action (min)[e]
3a[d]	i.v.: 40.1 (30.4–48.5)	>95	180
	p.o.: 77.0 (57.8–98.1)	100	>480
4a[d]	i.v.: 434 (347–499)	100	300
	p.o.: 1432 (1172–1758)	>95	>600
48a[c]	i.v.: 22.2 (18.0–27.6)	>95	n.d.
	p.o.: 3062 (2622–3538)	100	n.d.
fentanyl citrate	i.v.: 11.2 (8.5–15.1)	100	40
	p.o.: 1956 (1378–2797)	100	90
hydromorphone HCl	i.v.: 622 (529–778)	100	n.d.
	p.o.: 18753 (13466–25284)	>95	n.d.

[a]Hydrochloride. [b]Dihydrochloride. [c]Citrate. [d]Hemicitrate. [e]Duration of action was determined for a dose that produces approximately 90% MPE; it describes the duration for which the antinociceptive efficacy is >20% MPE. n.d. = not determined.

dx.doi.org/10.1021/ml500117c | ACS Med. Chem. Lett. 2014, 5, 857–862

Compound **4a** also exerted dose-dependent activity in the mouse tail-flick test (Figure 3), with ED_{50} values of 434 nmol/kg i.v. and 1432 nmol/kg p.o. This is about 10-fold less potent than **3a** after both i.v. and p.o. dosing, which can be clearly explained by the observed higher volume of distribution and clearance. The potency of **48a** after oral dosing was surprisingly low as compared to cebranopadol **3a** and could only be partially explained by its lower oral bioavailability (F = 14%).

A model of streptozotocin (STZ)-induced diabetic polyneuropathy was used to explore the efficacy of **3a** in a neuropathic pain state (see Supporting Information for details). A dose of 2.1 nmol/kg i.v. of **3a** was tested in STZ-treated diabetic CD-1 mice and, for comparison, in nondiabetic control animals. While **3a** induced a significant reduction of thermal hyperalgesia assessed in a hot plate test, it was without an antinociceptive effect in the control animals. The antihyperalgesic efficacy of 2.1 nmol/kg i.v. of **3a** was calculated to be 54.1% MPE (n = 10, SEM ± 4.6% MPE; $p < 0.001$ vs vehicle control) (Figure 4). Thus, in the neuropathic pain state, **3a**

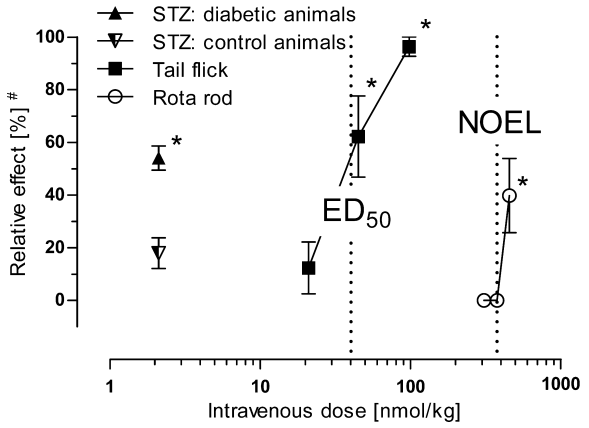

Figure 4. Dose-dependent effects of **3a** (cebranopadol) hemicitrate on heat nociception (tail-flick and hot plate in STZ control animals), on thermal hyperalgesia (hot plate in STZ diabetic animals), and on motor coordination (rota rod) after i.v. administration in mice. #, Relative effect refers to percentage of maximum possible effect (% MPE) for tail-flick and STZ models, or relative decrease in performance time on the rotating rod (rota rod). Error bars indicate SEM (n = 10). *, $p < 0.05$ versus vehicle control.

showed about half-maximum antihyperalgesic activity at a dose being 20 times lower than the ED_{50} value in the tail-flick model of acute nociception.

We decided to progress **3a**, due to its high efficacy and potency after oral and intravenous administration, for in-depth profiling. The cytochrom-P450 inhibition potential of **3a** was estimated after incubation with human CYP1A2, CYP2A6, CYP2B6, CYP2C8, CYP2C9, CYP2C19, CYP2D6, CYP2E1, or CYP3A4/5 and probe substrates selectively metabolized by these enzymes. None of the tested cytochrome P450 enzymes were inhibited in vitro by **3a** up to 250 nM.

The interaction of **3a** with safety-relevant cardiovascular targets was characterized: L-type Ca^{2+}-channel (benzothiazepine site) rat brain cortex K_i (μM) = 0.8 (N = 2); L-type Ca^{2+}-channel (phenylalkylamine site) rat brain cortex K_i (μM) = 0.48 (N = 2); L-type Ca^{2+}-channel (dihydropyridine site) rat whole brain K_i (μM) > 100 (N = 2); and *h*ERG channel human recombinant K_i (μM) > 100 (N = 2). Taking into account the high affinity of **3a** to interact with the primary targets (K_i < 1 nM), the affinities toward these safety relevant targets are expected to be without biological relevance. More detailed electrophysiological investigations using the whole-cell patch-clamp technique[12] revealed that **3a** did not affect *h*ERG-mediated potassium currents in transfected HEK293 cells up to 10 μM.

Having ensured a low potential to induce cardiac side effects by **3a** we embarked on assessing its side effects profile. Treatment with opioid drugs can be associated with severe side effects on the central nervous system (CNS) and gastrointestinal functions.[13]

In order to investigate its potential to affect the CNS, **3a** was investigated in a rota-rod test.[14] In male CD-1 mice, intravenous administration of **3a** at doses up to 376 nmol/kg did not significantly influence motor coordination in the rota-rod test. At a dose of 454 nmol/kg, **3a** induced a significant impairment of the rota-rod performance. The time that animals were able to remain on the rotating rod was shortened transiently for about 30−60 min after administration. The maximum effect was observed 15 min after administration, when the time on the rod was shortened from the maximum performance time of 120 s to 72 ± 17 s (mean ± SEM). Concurrently, the number of failures increased significantly up to 2.6 ± 0.9 (mean ± SEM). The no observed effect level (NOEL) for **3a** was therefore considered to be 376 nmol/kg. An ED_{50} value could not be calculated but is estimated to be >454 nmol/kg. Compound **3a** is, thus, characterized by a safety margin ≥10-fold between the ED_{50} value in the tail-flick test and the NOEL for effects on motor coordination (Figure 4). This is in clear contrast to standard opioids such as morphine or oxycodone that impair motor coordination within the antinociceptive dose range.[15]

Effects of **3a** on the gastrointestinal system were investigated in the charcoal transit test in male NMRI mice.[16] In this assay, effects on gut motility were measured as changes in transit rate of an orally administered charcoal suspension. Intravenous administration of **3a** at doses between 10 and 454 nmol/kg induced a dose-dependent inhibition of intestinal charcoal transit. NOEL was 21 nmol/kg i.v., and the ED_{50} was 87 nmol/kg i.v. A comparison of this ED_{50} value to the ED_{50} value in the mouse tail-flick assay points toward a separation of the analgesic dose range from doses inhibiting gastrointestinal motility. In contrast to standard opiates like morphine, which inhibits intestinal transit in mice already at doses below the ED_{50} in the tail-flick assay,[16,17] **3a** clearly showed effects on gut motility at doses higher than those required to induce antinociception.

In summary, **3a** (cebranopadol) exhibited high efficacy in a mouse model of acute pain with a potency comparable to the strong opioid fentanyl. In a model of polyneuropathic pain, **3a** (cebranopadol) showed an about 20 times higher potency as compared to the acute pain model. In contrast to standard opioids, which induce marked CNS side effects and inhibition of gastrointestinal transit at doses below or within the half-maximum effective analgesic dose range,[17,18] **3a** (cebranopadol) exhibits distinctly improved margins between the analgesic dose range and doses inducing significant gastrointestinal or CNS side effects, which point towards a broader therapeutic window (Figure 4).

A more detailed investigation of cebranopadol's pharmacological profile has been published elsewhere.[9] Currently, cebranopadol is in clinical development for the treatment of severe chronic nociceptive and neuropathic pain.

dx.doi.org/10.1021/ml500117c | ACS Med. Chem. Lett. 2014, 5, 857−862

■ ASSOCIATED CONTENT

Supporting Information

Assay description and experimental procedures for the synthesis and characterization of selected compounds. This material is available free of charge via the Internet at http://pubs.acs.org.

■ AUTHOR INFORMATION

Corresponding Author

*(S.S.) E-mail: stefan.schunk@grunenthal.com.

Notes

The authors declare no competing financial interest.

■ ACKNOWLEDGMENTS

We would like to thank H. Steinhagen, P. Ratcliffe, S. Frosch, and E. Hoppe for very helpful discussions, F. Theil (ASCA GmbH) for conception and realization of compounds, T. Koch for obtaining NOP and MOP receptor binding data,and S. Brenner, P. Günther, B. Liebenhoff, M. Mülfarth, and R. Woloszczak for technical assistance with the in vivo experiments. Detailed 1H and NOE NMR analysis for determination of stereochemical configuration by P. Jonas and M. Schade, high-resolution mass by J. Bergstreiser and M. Fuhr, and eADME characterization by S. Steufmehl are greatly acknowledged.

■ ABBREVIATIONS

CHO, Chinese hamster ovary cells; CI, confidence interval; CNS, central nervous system; DOP, delta opioid peptide; EC_{50}, concentration with half-maximum inducible [^{35}S]GTPγS binding; ED_{50}, half-maximum effective dose; E_{max}, maximum possible effect for the agonist; GTPγS, guanosine-5′-[γ-thio]triphosphate; *h*NOPr, Human nociceptin/orphanin FQ receptor; *h*MOPr, Human μ opioid receptor; HCl, hydrochloride; IC_{50}, half-maximum inhibitory concentration; i.v., intravenous; K_i, dissociation constant for inhibitor binding; KOP, kappa opioid peptide; MeCN, acetonitrile; MOP, mu opioid peptide; MPE, maximum possible effect; NOEL, no observed effect level; NOP, nociceptin/orphanin FQ peptide; SNL, spinal nerve ligation; TES, triethylsilyl

■ REFERENCES

(1) Cremeans, C. M.; Gruley, E.; Kyle, D. J.; Ko, M.-C. Roles of μ-opioid receptors and nociceptin/orphanin FQ peptide receptors in buprenorphine-induced physiological responses in primates. *J. Pharmacol. Exp. Ther.* **2012**, *343*, 72−81.

(2) Toll, L. The use of bifunctional NOP/Mu and NOP receptor selective compounds for the treatment of pain, drug abuse, and psychiatric disorders. *Curr. Pharm. Des.* **2013**, *19*, 7451−60.

(3) Schunk, S.; Linz, K.; Hinze, C.; Frormann, S.; Oberbörsch, S.; Sundermann, B.; Zemolka, S.; Englberger, W.; Germann, T.; Kless, A.; Christoph, T.; Kögel, B. Y.; Schröder, W.; Harlfinger, S.; Saunders, D.; Sonnenschein, H. Discovery of spiro[cyclohexane-dihydropyrano[3,4-b]indole]-amines as potent NOP and opioid receptor agonists. *ACS Med. Chem. Lett.* **2014**, DOI: 10.1021/ml500116x.

(4) Larock, R. C.; Yum, E. K. Synthesis of indoles via palladium-catalyzed heteroannulation of internal alkynes. *J. Am. Chem. Soc.* **1991**, *113*, 6689−90.

(5) Hinze, C.; Aulenbacher, O.; Sundermann, B.; Oberboersch, S.; Friderichs, E.; Englberger, W.; Koegel, B.-Y.; Linz, K.; Schick, H.; Sonnenschein, H.; Henkel, B.; Rose, V. S.; Lipkin, M. J. Preparation of spirocyclic indoles as ORL-1 receptor ligands for the treatment of pain. U.S. Patent 8,053,576, Nov 8, 2011.

(6) Thompson, A. A.; Liu, W.; Chun, E.; Katritch, V.; Wu, H.; Vardy, E.; Huang, X.-P.; Trapella, C.; Guerrini, R.; Calo, G.; Roth, B. L.; Cherezov, V.; Stevens, R. C. Structure of the nociceptin/orphanin FQ receptor in complex with a peptide mimetic. *Nature* **2012**, *485*, 395−399.

(7) Manglik, A.; Kruse, A. C.; Kobilka, T. S.; Thian, F. S.; Mathiesen, J. M.; Sunahara, R. K.; Pardo, L.; Weis, W. I.; Kobilka, B. K.; Granier, S. Crystal structure of the μ-opioid receptor bound to a morphinan antagonist. *Nature* **2012**, *485*, 321−326.

(8) Standard modeling techniques have been applied to dock, optimize, and visualize the binding modes of our compounds as implemented in MOE2012.10 (Molecular Operating Environment 2012, CCG, Montreal, Canada).

(9) Linz, K.; Christoph, T.; Tzschentke, T. M.; Koch, T.; Schiene, K.; Gautrois, M.; Schröder, W.; Kögel, B. Y.; Beier, H.; Englberger, W.; Schunk, S.; De Vry, J.; Jahnel, U.; Frosch, S. Cebranopadol: A novel potent analgesic nociceptin/orphanin FQ peptide and opioid receptor agonist. *J. Pharmacol. Exp. Ther.* **2014**, *349*, 535−548.

(10) D'Amour, F. E.; Smith, D. L. A method for determining loss of pain sensation. *J. Pharmacol. Exp. Ther.* **1941**, *72*, 74−79.

(11) Terlinden, R.; Kogel, B. Y.; Englberger, W.; Tzschentke, T.M. In vitro and in vivo characterization of tapentadol metabolites. *Methods Find. Exp. Clin. Pharmacol.* **2010**, *32*, 31−38.

(12) Hamill, O. P.; Marty, A.; Neher, E.; Sakmann, B.; Sigworth, F. J. Improved patch-clamp techniques for high-resolution current recording from cells and cell-free membrane patches. *Pflügers Arch.* **1981**, *391*, 85−100.

(13) Zöllner, C.; Stein, C. Opioids. *Handb. Exp. Pharmacol.* **2007**, 31−63.

(14) Dunham, N. W.; Miya, T. S. A note on a simple apparatus for detecting neurological deficits in rats and mice. *J. Am. Pharm. Assoc.* **1957**, *46*, 208−209.

(15) Winter, L.; Nadeson, R.; Tucker, A. P.; Goodchild, C. S. Antinociceptive properties of neurosteroids: A comparison of alphadolone and alphaxalone in potentiation of opioid antinociception. *Anesth. Analg.* **2003**, *97*, 798−805.

(16) Niemegeers, C. J. E.; Lenaerts, F. M.; Janssen, P. A. J. Loperamide (R 18553), a novel type of antidiarrheal agent. Part 2: In vivo parenteral pharmacology and acute toxicity in mice. Comparison with morphine, codeine and diphenoxylate. *Arzneimittelforschung* **1974**, *24*, 1636−1641.

(17) Tzschentke, T. M.; de Vry, J.; Terlinden, R.; Hennies, H. H.; Lange, C.; Strassburger, W.; Haurand, M.; Kolb, J.; Schneider, J.; Buschmann, H.; Finkam, M.; Jahnel, U.; Friderichs, E. Tapentadol hydrochloride. Analgesic, mu-opioid receptor agonist, noradrenaline reuptake inhibitor. *Drugs Future* **2006**, *31*, 1053−1061.

(18) Meert, T. F.; Vermeirsch, H. A. A preclinical comparison between different opioids: antinociceptive versus adverse effects. *Pharmacol., Biochem. Behav.* **2005**, *80*, 309−326.